Physicochemical Properties of Nanoparticles Regulate Translocation across Pulmonary Surfactant Monolayer and Formation of Lipoprotein Corona

Supplementary Information

Guoqing Hu[1]*, Bao Jiao[1], Xinghua Shi[1], Russell P. Valle[2], Qihui Fan[2], and Yi Y. Zuo[2]*

1. The State Key Laboratory of Nonlinear Mechanics (LNM), Institute of Mechanics, Chinese Academy of Sciences, Beijing, 100190, China

2. Department of Mechanical Engineering, University of Hawaii at Manoa, Honolulu, HI, 96822

* e-mail: guoqing.hu@imech.ac.cn; yzuo@hawaii.edu

S1. Additional experimental data

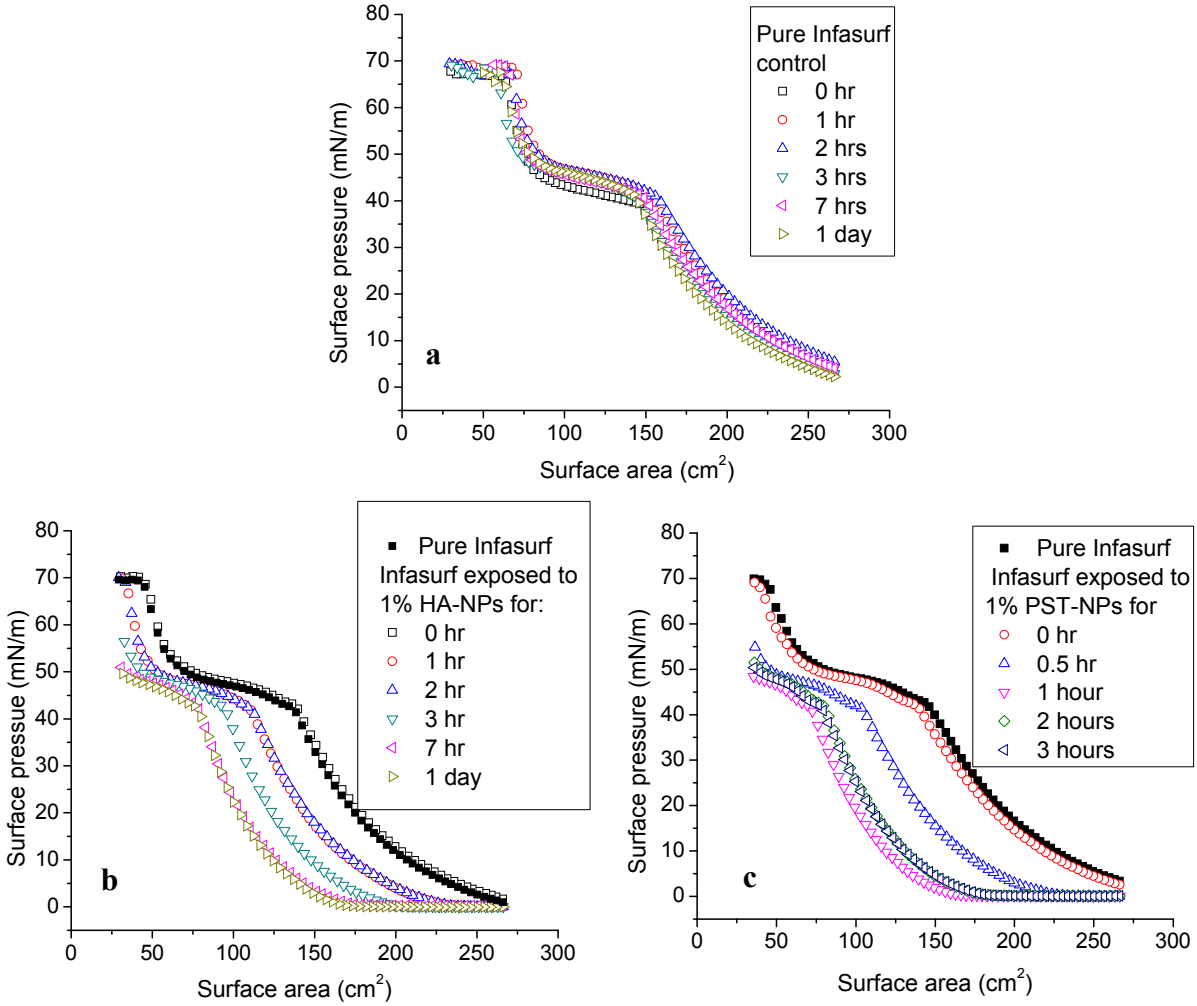

Figure S1. Time-dependent inhibition of Infasurf films by NPs of different hydrophobicity. **a,** Control experiment: time-dependent compression isotherms of pure Infasurf. Pure Infasurf is very stable, indicated by consistent compression isotherms without time-dependent shifting.[1] **b,** Infasurf exposed to 50 µg/mL (i.e., 1% surfactant phospholipids) hydrophilic hydroxyapatite NPs (HA-NPs) shows time-dependent inhibition, indicated by isotherm shifting to the left. Surfactant inhibition stabilizes after 7 hours of particle exposure.[1] **c,** Infasurf exposed to 50 µg/mL hydrophobic polystyrene NPs (PST-NPs) stabilizes after 1 hour of particle exposure. This comparison demonstrates the effect of particle hydrophobicity on kinetics of surfactant inhibition. The hydrophobic NPs tend to inhibit pulmonary surfactant much quicker than hydrophilic NPs.

S2. Detailed molecular dynamics simulations

S2.1. Overall system setup

As shown in Fig. S2, our initial simulation system consisted of a water slab sandwiched by two symmetric pulmonary surfactant monolayers. The water slab was set to be 20 nm in thickness (approximately 10 times the thickness of a lipid monolayer), large enough to separate the two monolayers without interaction with each other. In other words, during our simulations these two leaflets behaved as independent monolayers instead of a bilayer. Single nanoparticles were introduced symmetrically from the airside modeled by a vacuum. This symmetric arrangement allows us to conveniently set up system boundaries without compromising the accuracy of simulating monolayers or significantly increasing the computational load. Only the top leaflet (at $z=0$) of these two monolayers was illustrated in the paper. To study translocation of nanoparticles across static monolayers (Fig. 2), the system was studied within a simulation box with a constant volume and constant surface area of the monolayer. To simulate interactions between nanoparticles and dynamic pulmonary surfactant monolayers (Figs. 3-5), the simulation box and the surface area of the monolayers were compressed.

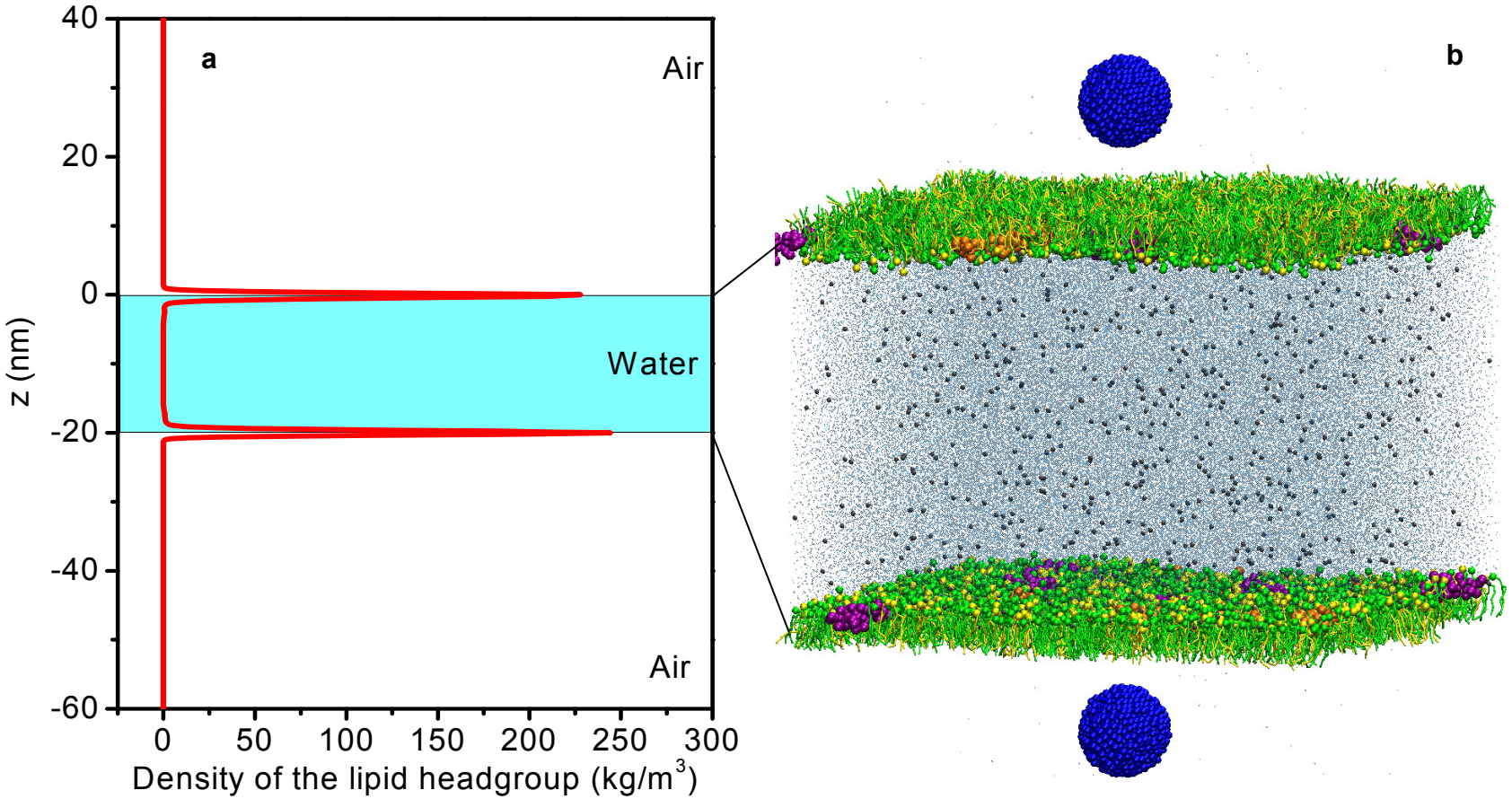

Figure S2. Initial setup of the molecular dynamics simulation system. a, The initial density profile of lipid headgroups along the vertical direction of the simulation box; **b,** The simulated symmetric system with a water slab sandwiched by two non-interacting surfactant monolayers with individual nanoparticles introduced from the airside.

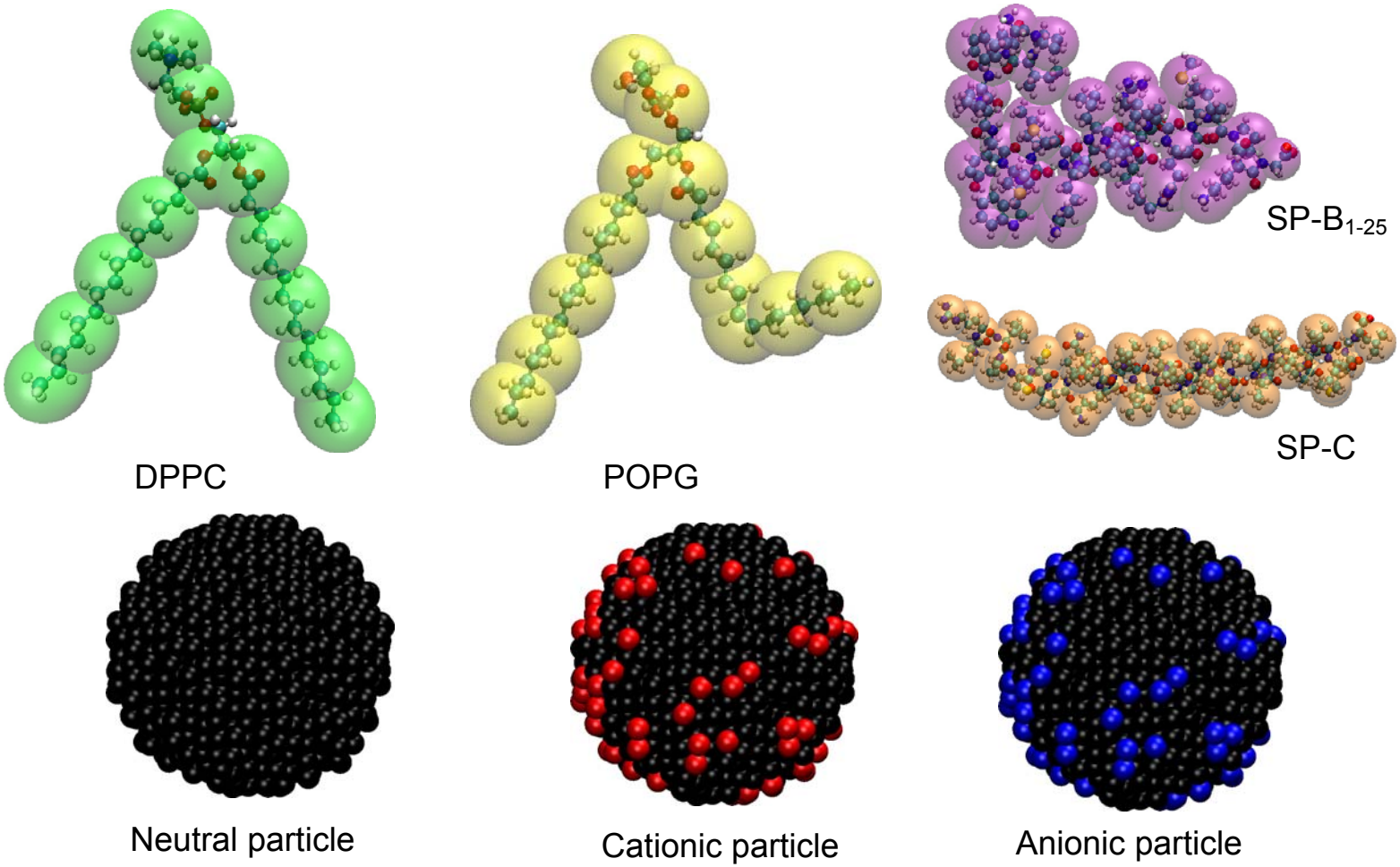

Figure S3. Schematics of coarse-grained (CG) molecules and nanoparticles involved in our simulations. DPPC in green; POPG in yellow; SP-B_{1-25} in purple; SP-C in orange; neutral particle in black. Surface of the cationic particle was modified with randomly distributed positive charges shown in red. Surface of the anionic particle was modified with randomly distributed negative charges shown in blue. For clarification, cationic and anionic particles in text are shown in solid red and solid blue, respectively.

S2.2. Coarse-grained models

The entire system was simulated with coarse-grained (CG) models which allow molecular simulations at a larger length-scale and longer time-scale than all-atom models. Each pulmonary surfactant monolayer contained 1,120 CG DPPC (green) and 480 CG POPG (yellow) molecules (7:3), doped with 7 CG SP-B_{1-25} (purple) and 7 CG SP-C (orange) molecules. The simulation parameters of CG DPPC and CG POPG were taken from the MARTINI force field.[2-4] All-atom models for SP-C (1SPF.pdb) and SP-B_{1-25} (1DFW.pdb) were obtained from the protein data bank.[5] CG models of these two protein peptides were derived from these all-atom models using martinize.py by analyzing the secondary structure and the sequence of residues of these protein peptides.

The CG models for nanoparticles were built to be compatible with the MARTINI CG force field for proteins and lipids.[2-4] Each nanoparticle contained 1,721 CG beads arranged in a face-centered cubic arrangement. The diameter of the final nanoparticle was approximately 5 nm. The CG bead types P2 and C1 were used for constructing the neutral (black) hydrophilic and hydrophobic nanoparticles, respectively. Qda and Qa were used to modify the surface charges of the particle. Cationic particle was shown in red and anionic particle was shown in blue. The water slab contained 158,418 CG water beads and 862 Na^+ ions to neutralize the system.

Fig. S3 shows the schematics and color schemes of the simulated CG molecules and particles.

S1.3. Molecular dynamics simulations

All simulations were performed using the GROMACS 4.5.4.[6] All simulations were conducted at a constant temperature of 310 K. For the study of particle translocation across a static surfactant monolayer (Fig. 2), the simulation box was set to be at a constant volume of 31 $\times$31$\times$100 nm, at which the surfactant monolayer had a molecular area of approximately 60 $Å^2$

per lipid. The nanoparticle (NP) was introduced to the pre-equilibrium monolayer and the interaction was simulated up to 200 ns. The potential of mean force (PMF) was calculated using the weighted histogram analysis method (WHAM) [7] and the umbrella sampling technique [8] with 0.2 nm spacing between the umbrella windows. For each window the system underwent 20 ns constant volume and temperature equilibration simulations and 50 ns umbrella sampling runs.

For the study of particle interaction with dynamic surfactant film (Figs. 3-5), the simulation box and the surface area of the monolayers were compressed by applying positive lateral pressure using the semi-isotropic pressure coupling scheme (isotropic coupling in the x-y plane and anisotropic coupling in the z-direction). The Berendsen barostat was used for the semi-isotropic pressure coupling with a coupling constant $\tau_P = 4$ ps. The system compressibility was set to be 5×10^{-5} bar^{-1} in the x-y plane and 0 bar^{-1} in the z-direction. The temperature was maintained at 310 K by Berendsen temperature coupling with a coupling constant $\tau_T = 1$ ps. The time step was 20 fs and the neighbor list was updated every 10 steps.

S3. Interactions between the cationic hydrophilic NP and lipids

For the hydrophilic NPs, we found that the cationic NP selectively adsorbs POPG. Fig. S4 shows the molar ratio of POPG to DPPC lipids adsorbed onto the NP surface. A higher POPG:DPPC ratio is found in the lipid monolayer adsorbed on the particle surface than that of the interfacial monolayer (POPG:DPPC=3:7). This is likely due to electrostatic interactions between the cationic NP and the anionic POPG molecules.

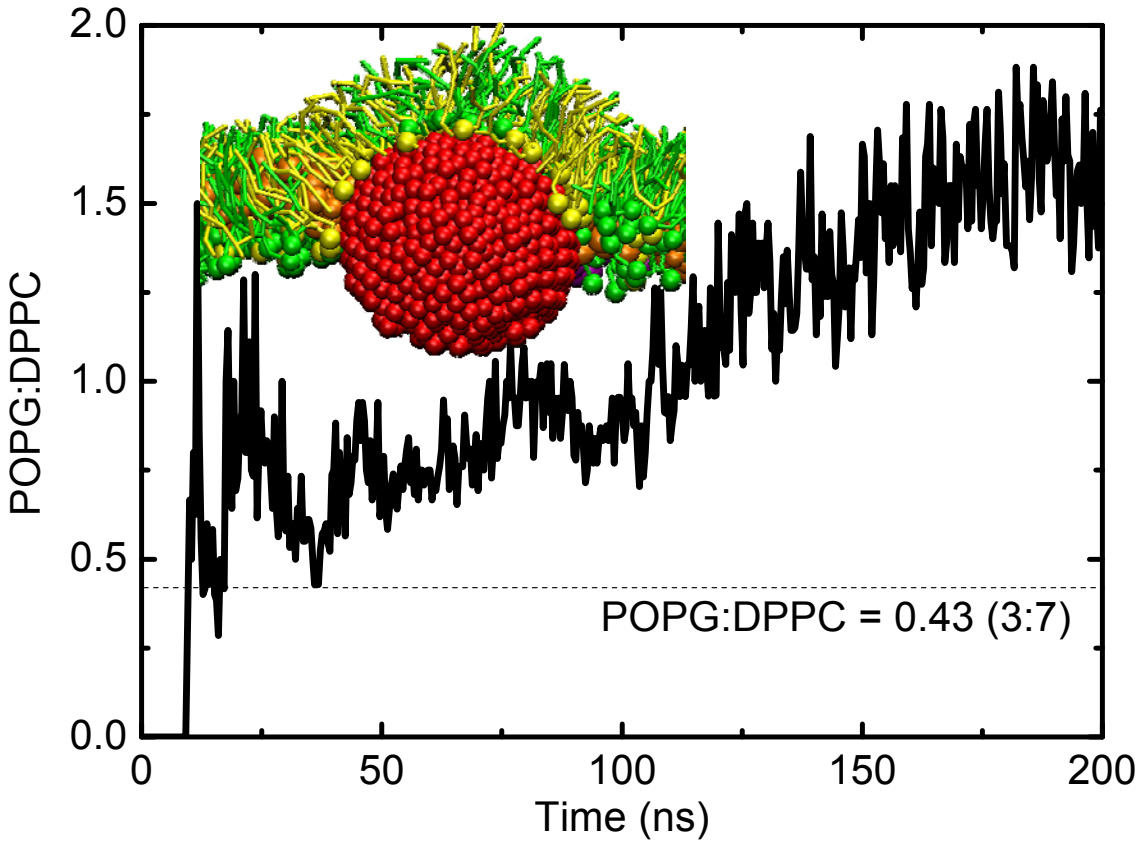

Figure S4. Time dependent variations of POPG:DPPC molecular ratio adsorbed on the surface of a cationic hydrophilic NP.

S4. Interactions between the anionic hydrophilic NP and surfactant proteins

To study the binding specificity between the anionic hydrophilic NP and the protein molecules, Fig. S5a shows the interaction distance between the NP and the protein molecules (SP-B_{1-25} and SP-C) during the simulation time. It is found that SP-B_{1-25} selectively binds to the NP. However, despite being in contact with the NP from 25 to 125 ns, SP-C is eventually separated from the NP at equilibrium. Similarly, Fig. S5b shows the potential of mean force (PMF) required to "pull" a protein molecule out of the interfacial surfactant monolayer. It is found that the PMF of "pulling" a SP-C molecule is more than double of the PMF of "pulling" a SP-B_{1-25} molecule, indicating a higher affinity between the surfactant monolayer and the SP-C molecule than with the SP-B_{1-25} molecule.

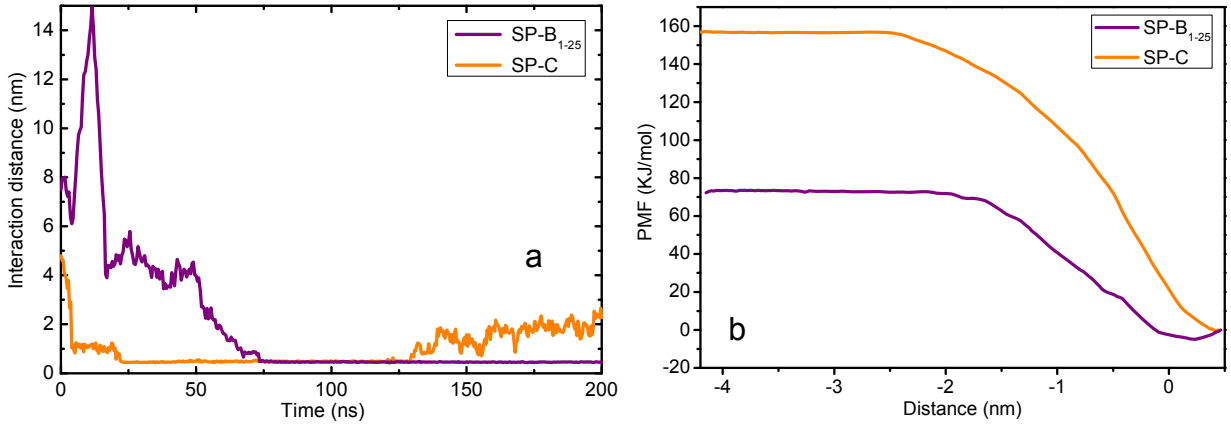

Figure S5. Additional MD simulations that confirm the binding specificity between an anionic hydrophilic NP and surfactant proteins (SP-B_{1-25} and SP-C). a, Interaction distance as a function of the simulation time; **b,** Potential of mean force (PMF) for interaction between the surfactant monolayer and the protein molecules.

S5. Amino acid sequences of SP-B_{1-25} and SP-C

The human SP-B monomer contains 79 amino acids. The detailed three dimensional structure of this protein is still unclear. In our MD simulations, we used SP-B_{1-25}, which is a SP-B peptide of 1-25 amino-terminal residues, to replace SP-B. Despite the simplicity, both experimental [9-15] and MD studies [16-18] have shown that SP-B_{1-25} represents certain properties of the full-length SP-B.

Fig. S6. compares the charge and polarity of amino acid sequences for SP-B_{1-25} and SP-C. SP-B_{1-25} contain 4 net positive changes and 16 non-polar amino acids out of the 25 amino acid residue. The human SP-C consists of 35 amino-acid polypeptide enriched in valine (V), leucine (L), and isoleucine (I), which make SP-C one of the most hydrophobic proteins in the proteome. Specifically, SP-C contains 3 net positive charges and 27 non-polar amino acids out of the 35 amino acid residue. Hence, compared to SP-C, SP-B_{1-25} has a higher positive charge density and is significantly less hydrophobic.

a. SP-B_{1-25}

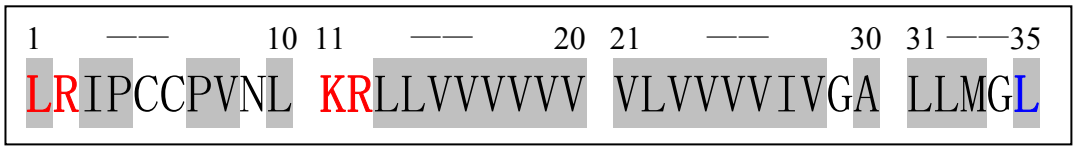

b. SP-C

Figure S6. Amino acid sequence of a. SP-B_{1-25}; and b. SP-C molecules. For each amino acid, the charge at pH 7 is indicated by different colors: positive (red), negative (blue), and neutral (black); the polarity is indicated by the background: polar (clear) and non-polar (gray).

References

1. Fan, Q.; Wang, Y. E.; Zhao, X.; Loo, J. S.; Zuo, Y. Y. Adverse Biophysical Effects of Hydroxyapatite Nanoparticles on Natural Pulmonary Surfactant. *ACS. Nano.* **2011**, *5*, 6410-6416.
2. Marrink, S. J.; de Vries, A. H.; Mark, A. E., Coarse Grained Model for Semiquantitative Lipid Simulations. *J. Phys. Chem. B.* **2004**, *108*, 750-760.
3. Marrink, S. J.; Risselada, H. J.; Yefimov, S.; Tieleman, D. P.; De Vries, A. H. The MARTINI Force Field: Coarse Grained Model for Biomolecular Simulations. *J. Phys. Chem. B.* **2007**, *111*, 7812-7824.
4. Monticelli, L.; Kandasamy, S. K.; Periole, X.; Larson, R. G.; Tieleman, D. P.; Marrink, S. J. The MARTINI Coarse-Grained Force Field: Extension to Proteins. *J. Chem. Theory Comput.* **2008**, *4*, 819-834.
5. Berman, H. M.; Westbrook, J.; Feng, Z.; Gilliland, G.; Bhat, T.; Weissig, H.; Shindyalov, I. N.; Bourne, P. E. The Protein Data Bank. *Nucleic Acids Res.* **2000**, *28*, 235-242.
6. Lindahl, E.; Hess, B.; van der Spoel, D. GROMACS 3.0: A Package for Molecular Simulation and Trajectory Analysis. *J. Mol. Model.* **2001**, *7*, 306-317.
7. Kumar, S.; Rosenberg, J. M.; Bouzida, D.; Swendsen, R. H.; Kollman, P. A. The Weighted Histogram Analysis Method for Free‐Energy Calculations on Biomolecules. I. The Method. *J. Comput. Chem.* **1992**, *13*, 1011-1021.
8. Torrie, G.; Valleau, J. Nonphysical Sampling Distributions in Monte Carlo Free-Energy Estimation: Umbrella Sampling. *J. Comput. Phys.* **1977**, *23*, 187-199.
9. Farver, R. S.; Mills, F. D.; Antharam, V. C.; Chebukati, J. N.; Fanucci, G. E.; Long, J. R. Lipid Polymorphism Induced by Surfactant Peptide SP-B(1-25). *Biophys. J.* **2010**, *99*, 1773-1782.
10. Longo, M.; Bisagno, A.; Zasadzinski, J.; Bruni, R.; Waring, A. A Function of Lung Surfactant Protein SP-B. *Science.* **1993**, *261*, 453-456.
11. Lee, K. Y. C.; Lipp, M. M.; Zasadzinski, J. A.; Waring, A. J. Effects of Lung Surfactant Specific Protein SP-B and Model SP-B Peptide on Lipid Monolayers at the Air-Water Interface. *Colloids Surf., A.* **1997**, *128*, 225-242.
12. Veldhuizen, E. J. A.; Waring, A. J.; Walther, F. J.; Batenburg, J. J.; van Golde, L. M. G.; Haagsman, H. P. Dimeric N-terminal Segment of Human Surfactant Protein B (dSP-B1-25) Has Enhanced Surface Properties Compared to Monomeric SP-B1-25. *Biophys. J.* **2000**, *79*, 377-384.
13. Gupta, M.; Hernandez-Juviel, J.; Waring, A.; Bruni, R.; Walther, F. Comparison of Functional Efficacy of Surfactant Protein B Analogues in Lavaged Rats. *Eur.Respir. J.* **2000**, *16*, 1129-1133.
14. Gupta, M.; Hernandez-Juviel, J.; Waring, A.; Walther, F. Function and Inhibition Sensitivity of the N-terminal Segment of Surfactant Protein B (SP-B1-25) in Preterm Rabbits. *Thorax.* **2001**, *56*, 871-876.
15. Flanders, B. N.; Vickery, S. A.; Dunn, R. C. Divergent Fluctuations in the Molar Area of a Model Lung Surfactant. *J. Phys. Chem. B.* **2002**, *106*, 3530-3533.
16. Choe, S.; Chang, R.; Jeon, J.; Violi, A. Molecular Dynamics Simulation Study of a Pulmonary Surfactant Film Interacting with a Carbonaceous Nanoparticle. *Biophys. J.* **2008**, *95*, 4102-4114.
17. Freites, J. A.; Choi, Y.; Tobias, D. J. Molecular Dynamics Simulations of a Pulmonary Surfactant Protein B Peptide in a Lipid Monolayer. *Biophys. J.* **2003**, *84*, 2169-2180.

18. Kaznessis, Y. N.; Kim, S.; Larson, R. G. Specific Mode of Interaction Between Components of Model Pulmonary Surfactants Using Computer Simulations. *J. Mol. Biol.* **2002**, *322*, 569-582.